IEEE Access
Multidisciplinary | Rapid Review | Open Access Journal

Received 15 December 2023, accepted 4 January 2024, date of publication 9 January 2024, date of current version 29 January 2024.

Digital Object Identifier 10.1109/ACCESS.2024.3351883

RESEARCH ARTICLE

Computer Aided Cervical Cancer Diagnosis Using Gazelle Optimization Algorithm With Deep Learning Model

MOHAMED K. NOUR[1], (Member, IEEE), IMÈNE ISSAOUI[2], ALAA EDRIS[3], AHMED MAHMUD[4], MOHAMMED ASSIRI[5], AND SARA SAADELDEEN IBRAHIM[5]

[1]Department of Computer Science, College of Computing and Information Systems, Umm Al-Qura University, Makkah 21421, Saudi Arabia
[2]Unit of Scientific Research, Applied College, Qassim University, Buraydah 52571, Saudi Arabia
[3]Department of Computer Science and Artificial Intelligence, College of Computer Science and Engineering, University of Jeddah, Jeddah 23890, Saudi Arabia
[4]Research Center, Future University in Egypt, New Cairo 11835, Egypt
[5]Department of Computer Science, College of Sciences and Humanities—Aflaj, Prince Sattam bin Abdulaziz University, Aflaj 16273, Saudi Arabia

Corresponding author: Mohamed K. Nour (mknour@uqu.edu.sa)

This study is partially funded by the Future University in Egypt (FUE).

ABSTRACT Cervical cancer (CC), the most common cancer among women, is most commonly diagnosed through Pap smears, a crucial screening process that includes collecting cervical cells for examination. Artificial intelligence (AI)-powered computer-aided diagnoses (CAD) system becomes a promising tool for improving CC diagnosis. Deep learning (DL), a branch of AI, holds particular potential in CAD systems for early detection and accurate diagnosis. DL algorithm is trained to identify abnormalities and patterns in Pap smear images, such as dysplasia, cellular changes, and other markers of CC. So, this study presents a Computer Aided Cervical Cancer Diagnosis utilizing the Gazelle Optimizer Algorithm with Deep Learning (CACCD-GOADL) model on Pap smear images. The foremost objective of the CACCD-GOADL approach is to examine the image detection of CC. To accomplish this, the CACCD-GOADL methodology uses an improved MobileNetv3 model for extracting complex patterns in Pap smear images. In addition, the CACCD-GOADL technique designs a new GOA for the hyperparameter tuning of the improved MobileNetv3 system. For the classification and identification of cancer, the CACCD-GOADL technique uses a stacked extreme learning machine (SELM) methodology. The simulation validation of the CACCD-GOADL approach is verified on a benchmark dataset of Herlev. Experimental results highlighted that the CACCD-GOADL algorithm reaches superior outcomes over other methods.

INDEX TERMS Cervical cancer, gazelle optimization algorithm, computer-aided diagnosis, deep learning, machine learning.

I. INTRODUCTION

Cervical cancer (CC) is a common cancer for females globally. Owing to the combination of high human papillomaviruses (HPV) in the host genome, CC occurs [1]. Nearly 99 % of CC cases are infected with a high risk of HPV that is transferred via sexual content. That is why an early recognition of CC has become vital for the well-organized management of patients clinically [2]. The highest challenge is changing biological information into valued knowledge. Normally, the improvement of CC is very slow as well as preceded by anomalies in the cervix (dysplasia). Moreover, the early-stage symptoms absence may cause a lack of attention to prevention [3], [4]. In addition to that, in many developing countries resources are absent so that the patients have poor obedience to routine screening due to low difficulty awareness. Even though there are severe medical and scientific developments, CC disease is not curable completely particularly if identified in a progressing stage. Prevention as well as screening services, plays an important role in the battle besides CC [5]. The CC screening comes with a common workflow such as cytology or PAP smear testing,

The associate editor coordinating the review of this manuscript and approving it for publication was Bing Li.

biopsy, HPV testing, and colposcopy. Many tools have sustained the workflow that is mainly produced to make it more low-cost, practical, and effectual [2], [6]. The PAP smear image screening is highly utilized for CC but it requires huge numbers of tiny analyses to identify cancer and non-cancer patients. The main goal of an automated PAP-smear study is to divide and then categorize CC in the pap-smear images as normal or abnormal [1]. The growth of such methods as Machine Learning (ML) and Medical Imaging (MI), in these studies, is a realism that aids in decreasing the time consumed as well as enhancing the exactness of cytologists' execution slide examination at the time of pap screening procedure.

The medical image investigation contains both methods as well as procedures to get full detailed data from the medical images for medical examination and involvement [7]. The ML method is the main branch of AI which shares the learning problems from data samples. ML uses a variety of optimization, probabilistic, and statistical approaches that permit computer networks to ''learn'' from previous samples as well as to identify hard-to-discern forms from complex, noisy, or large difficult databases [8]. ML and MI methods spontaneously analyze pap-smear images and then create the screening procedure quicker and more trustworthy [8]. Deep Learning (DL) techniques have become one of the popular tools for cancer study recently [9]. These models are capable of recognizing designs and difficult relationships from obtainable multimodal datasets for effective prediction of CC [10]. By considering the most important growth in demand for personalized treatment and then developments in DL models, hereby we analyze improvements in modern DL approaches for CC prediction and diagnosis [11].

This study presents a Computer Aided Cervical Cancer Diagnosis using the Gazelle Optimizer Algorithm with DL (CACCD-GOADL) approach on pap smear images. The main goal of the CACCD-GOADL approach is to examine the images for the detection of CC. To accomplish this, the CACCD-GOADL technique uses an improved MobileNetv3 model for extracting complex patterns in the pap smear images. In addition, the CACCD-GOADL technique designs a new GOA for the hyperparameter tuning of the improved MobileNetv3 methodology. For the classification and identification of cancer, the CACCD-GOADL technique uses a stacked extreme learning machine (SELM) method. The simulation validation of the CACCD-GOADL approach is tested on a benchmark dataset of Herlev. The major contribution of the study is listed as follows.

- Develops a new CACCD-GODL method for CC diagnosis, which is a cutting-edge fusion of nature-inspired optimization technique to improve the performance of the DL algorithm.
- Employs an enhanced MobileNetv3 model to extract complicated patterns in Pap smear images. This illustrates a strategic choice for the effective extraction of deep features, crucial to capture complex features related to CC diagnoses.
- Introduces a new GOA variant particularly developed for tuning hyperparameters in the enhanced MobileNetv3 architecture. This contribution highlights the framework's commitment to optimizing model parameters for better generalization and accuracy.
- To further improve diagnostic abilities, CACCD-GOADL exploits the SELM method for the classification and detection of cancer. This stacking technique aims to enhance the reliability and robustness of the model's predictions.

II. RELATED WORKS

Waly et al. [12] presented an intelligent deep CNN for CC identification and detection (IDCNN-CDC) technique employing bio-medical pap smear images. The Tsallis entropy approach with the dragonfly optimizer (TE-DFO) model defines the image segmentation for appropriately recognizing the diseased regions. Then, the features extracted from SqueezeNet have been implemented into the weighted ELM classification method for diagnosing and classifying cervical tissues. In [13], an approach was developed that supports in identification and classification of the cancer employing the HOG extraction feature as well as categorizing it through ANN, KNN, and SVM. Şentürk and Süleyman [14] introduced a transfer learning (TL) based CC identification technique for earlier analysis. Pap smear images could be pre-processed with the help of a median filter (MF) before training the DL method to eliminate noise in the images for improving classification.

Suguna and Balamurugan [15] implemented a CAD for CC Screening utilizing Monarch Butterfly optimization with the DL (CADCCSMBODL) method. To remove features, this developed CADCCS-MBODL method exploits the EfficientNet framework with the MBO technique as a hyperparameter optimization. Then, the XGBoost algorithm was utilized to classify and identify the CC. In [16], an efficient hybrid DL approach employing Small Object Detection-GAN (SOD-GAN) with fine-tuned SAE (F-SAE) was designed to overcome the limitations aforementioned. The technique parameters could be utilizing F-SAE, and SOD-GAN hyperparameters must be enhanced and normalized for quickly diagnosing cancers. Al Masri and Mokayed [17] developed an intelligent ML-based CAD (IML-CAD) method for classifying CC. The IML-CAD algorithm includes various phases of processes for identifying and categorizing the malignant cervix cells. Besides, the least squares-SVM (LS-SVM) method and local binary patterns (LBP) based feature extractor are devised for classifying CC.

In [18], the authors presented a TL method of the InceptionV3 network for classifying moderately, good, and poorly distinguished cervical HI that can be marked by employing immunohistochemistry techniques. In this model, an InceptionV3-based TL algorithm was initially designed. Next, a fine-tuning method was implemented for extracting efficient DL features from the model. In [19], the authors designed a fully automatic pipeline for CC identification and

recognition from cervigram images. This introduced pipeline comprises 2 pre-trained DL methods for automatic CC classification and cervix identification. These features could be learned by applying 2 lightweight frameworks depending on CNN.

In [20], a medical image augmentation model such as texture-constrained multichannel progressive generative adversarial network (TMP-GAN) has been developed in this paper. TMP-GAN utilizes combined training of manifold networks to efficiently evade the classic defects of the present generation models. Zhou et al. [21] developed a dual-branch shape-aware network (DSANet) to divide the left ventricle, left atrium, and myocardium from the echocardiography. Wang et al. [22] main goal is to challenge the edema and scar segmentation from multiple-sequence CMR with an innovative auto-weighted supervision structure, where the connections between dissimilar supervised layers are discovered below a specific task objective by employing reinforcement learning.

III. THE PROPOSED MODEL

In this work, we have mainly concentrated on the design and growth of an automated CACCD-GOADL methodology for the identification and recognition of CC. The main intention of the CACCD-GOADL approach is to analyze the images for the detection of CC. To accomplish this, the CACCD-GOADL technique incorporates an improved MobileNetv3 model, GOA-based hyperparameter tuning, and SELM detection. Fig. 1 defines the workflow of the CACCD-GOADL method.

A. FEATURE EXTRACTION: IMPROVED MOBILENETV3 MODEL

For deriving feature vectors, the improved MobileNetv3 model can be used. MobileNet has lower latency and power, which is a small CV method design aimed to enhance accuracy but sufficiently the resource limitations of on-device or embedding apps [23]. Detection, segmentation, and classification tasks are executed utilizing these approaches, as with other large-scale methods. MobileNetV1 combined a novel feature named depth-wise discrete convolutional that radically decreases the count of essential parameters related to other designs that utilize even convolutions. The design of the MobileNetV1 technique comprises many depth-wise separable convolutional to reduce the operation counts needed by the model for backward and forward propagations. Standard convolution layers in CNNs treat all the channels similarly; but, SE blocks calculate the outcome by assuming the significance of all the channels.

Fig. 2 depicts the architecture of MobileNetV3. All the channels can initially compressed as one numeric value by SE block; then it is provided as a 2-layer feedforward network to measure the weight for all the channels. SE blocks can be executed similarly to the remaining layers for assigning distinct weights for many networks from the input once generating the resultant mapping feature, because it leads to enhanced accuracy. MobileNetV3 also establishes 2 developments with MobileNetV2 such as layer removal and employment of swish nonlinearity.

Layer removal: The 1×1 development layer, gained from the inverted remaining unit and conveyed beside the pooling layer from the final block of *MobileNetV*2, utilizes 1×1 mapping features instead of 7×7 mapping features, making it effectual for latency and computation. Therefore, the filtering and projection layers of the preceding bottleneck layer can removed.

Use of swish nonlinearity: Swish non-linearity can determined as:

$$swishx = x^{*}\sigma\,(x) \tag{1}$$

Swish non-linearity is established to improve accuracy. However, the MobileNetV3 creators exchanged the sigmoid function with hard swish for the sigmoid which is computational cost, and computational cost is decreased.

$$h - swish\,[x] = \frac{x^{*}\,(ReLU6\,(x+3))}{6} \tag{2}$$

B. PARAMETER TUNING: GOA

To adjust the hyperparameter values of the enhanced MobileNetv3 model, the GOA is applied. The GOA is a population-based optimizer approach that uses modified gazelles (X) randomly as searching agents [24]. The searching agent is indicated as a $n \times d$ matrix of the candidate solution. This method joins the lower bound (LB) and upper bound (UB) to describe the range of values for the population vector.

$$X = \begin{bmatrix} x_{1,1} & x_{1,2} & \cdots & x_{1,d-1} & x_{1,d} \\ x_{2,1} & x_{2,2} & \cdots & x_{2,d-1} & x_{2,d} \\ \vdots & \vdots & x_{i,j} & \vdots & \vdots \\ x_{n,1} & x_{n,2} & \cdots & x_{n,d-1} & x_{n,d} \end{bmatrix} \tag{3}$$

In Eq. (3), the matrix of the candidate population's location vector is X. The location vector (X) is randomly generated based on Eq. (4), where *rand* indicates the random integer, the upper and lower boundaries for the problems are UB_j and LB_j, correspondingly. n and d variables signify the number of gazelles and the dimension of search range, correspondingly.

$$x_{i,j} = rand \times \left(UB_j - LB_j\right) + LB_j \tag{4}$$

In all the iterations, $x_{i,j}$ create a solution candidate and the optimum solution attained is known as the minimal solution. The fittest or strongest gazelles have extraordinary capabilities in evading predators, spotting threats, and alerting others. Therefore, the optimal performance is nominated as a top gazelle and creates an Elite $n \times d$ matrix. This aids as a reference for the gazelles to define the next step at the searching stage.

$$Elite = \begin{bmatrix} x'_{1,1} & x'_{1,2} & \cdots & x'_{1,d-1} & x'_{1,d} \\ x'_{2,1} & x'_{2,2} & \cdots & x'_{2,d-1} & x'_{2,d} \\ \vdots & \vdots & x'_{i,j} & \vdots & \vdots \\ x'_{n,1} & x'_{n,2} & \cdots & x'_{n,d-1} & x'_{n,d} \end{bmatrix} \tag{5}$$

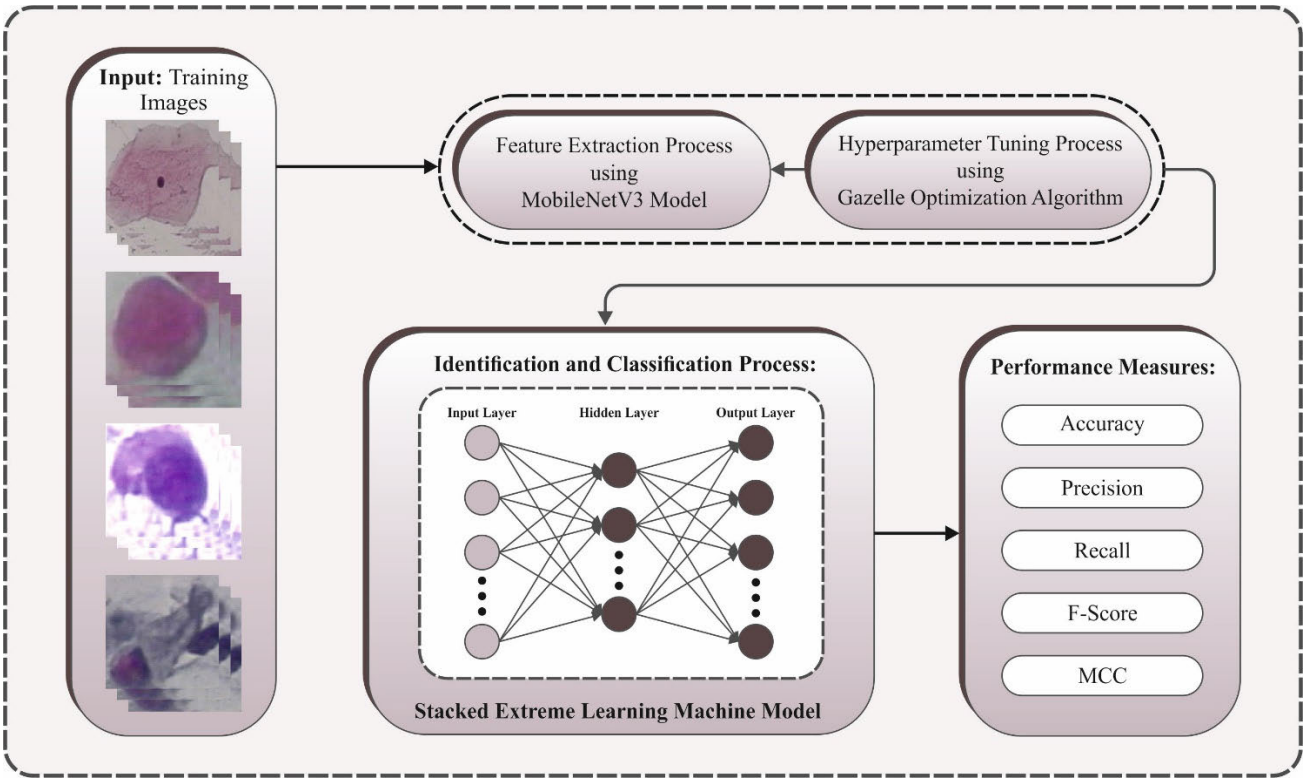

FIGURE 1. Workflow of the CACCD-GOADL approach.

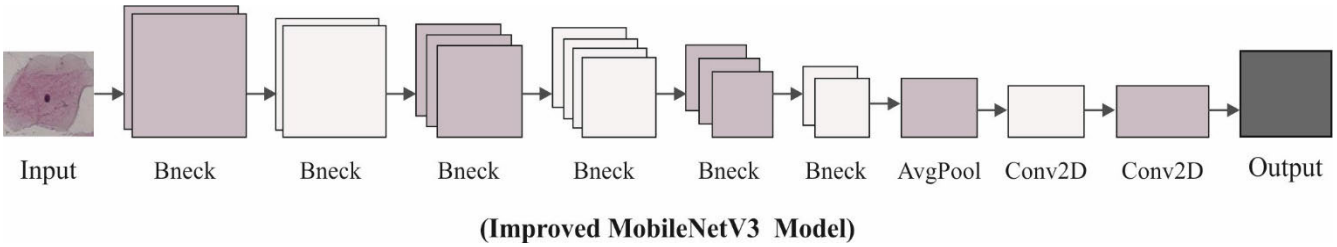

FIGURE 2. Structure of MobileNetV3.

In Eq. (5), the location vector of top gazelle is $x'_{i,j}$. GOA consider the predator and gazelle as searching agent as when the predator is identified, both parties flee in a similar way nearby safety. The predator discovers the search space as the gazelles escape. If the best gazelle replaces the top gazelle, the Elite matrix is updated at the iteration end.

The GOA stimulates the existence behaviors of gazelles, including browsing in the lack of hunters and flying to safer regions when a predator is spotted. Consequently, the optimizer method of the GOA is split into two different stages.

1) EXPLOITATION

The gazelles peaceably forage in the occurrence of a stalking predator or without a predator in the exploitation stage. The controlled Brownian movement with controlled and uniform steps is used for effectively exploring the neighboring area of the domain. During grazing, they move in a Brownian movement pattern. This behavior is expressed as follows.

$$gazelle_{i+1} = gazelle_i + s \cdot R * \cdot R_B * \cdot (Elite_i - R_B * \cdot gazelle_i) \tag{6}$$

In Eq. (6), the solution at next and existing iterations are $gazelle_{i+1}$ and $gazelle_i$. The foraging rapidity of the gazelles is the parameter s. R is a vector including uniformly distributed arbitrary number ranges within [0, 1]. R_B denotes the vector of arbitrary integers that simulates the Brownian movement.

2) EXPLORATION

When a predator is detected, the exploration stage begins. In responding to danger, gazelles show different behaviors namely foot stomping, tail flicking, or stotting up to the height of 2 m that ranges within [0,1]. Employing the Le'vy fight, the

gazelle responds primarily for its escape, but the hunter first utilizes the Brownian movement beforehand transitioning to the Le'vy fight. This behavior is expressed as follows:

$$\overrightarrow{gazelle_{i+1}} = \overrightarrow{gazelle_i} + S \cdot \mu \cdot \vec{R} * \cdot \vec{R_L} * \cdot \left(\overrightarrow{Elite_i} - \vec{R_L} * \cdot \overrightarrow{gazelle_i}\right) \quad (7)$$

where the top speed that gazelle could accomplish is S, a vector of arbitrary amounts according to Lévy distributions is $\rightarrow^{R_L}$. The chasing behaviors of predators can be mathematically modelled as follows:

$$\overrightarrow{gazelle_{i+1}} = \overrightarrow{gazelle_i} + S \cdot \mu \cdot CF * \cdot \vec{R_B} * \cdot \left(\overrightarrow{Elite_i} - \vec{R_L} * \cdot \overrightarrow{gazelle_i}\right) \quad (8)$$

In Eq. (8) the cumulative outcome of the predator is CF, evaluated by $CF = (1 - iter/iterMax)$. The effect of PSRs is modeled in Eq. (9).

$$\overrightarrow{gazelle_{i+1}} = \begin{cases} \overrightarrow{gazelle_i} + CF\left[\vec{LB} + \vec{R} * \cdot \left(\vec{UB} - \vec{LB}\right)\right] * \cdot \vec{U}; \\ \qquad ifr \leq PSRs \\ \overrightarrow{gazelle_i} + [PSRs\,(1-r) + r]\left(\overrightarrow{gazelle_{r1}} - \overrightarrow{gazelle_{r2}}\right) \\ \qquad ;else \end{cases} \quad (9)$$

where a binary vector created an arbitrary number r within [0, 1] is $\vec{U}$, thus $\vec{U} = 0$ for $r < 0.34$; or else $\vec{U} = 1$. random indexes of the gazelle matrix are $r1$ and $r2$.

The GOA approach improves an FF to achieve a better classifier result. It clarifies an optimistic integer for implying a good solution. In this case, the decreasing classifier rate of errors can be supposed to be the FF, as stated in Eq. (10).

$$\begin{aligned} fitness\,(x_i) &= ClassifierErrorRate\,(x_i) \\ &= \frac{No.ofmisclassifiedinstances}{Totalno.ofinstances} * 100 \end{aligned} \quad (10)$$

C. IMAGE CLASSIFICATION: SELM MODEL

For CC classification, the SELM model can be exploited. The ELM technique has been employed for resolving the single hidden-layer (HL) NN approach [25]. Typical NN learning approaches (like the BP technique) require obtaining a huge count of network-trained parameters and easily performing local optimum results. Accordingly, the ELM approach gets the benefits of quick learning speeds and optimum generalized ability. An FFNN with L hidden layer nodes can expressed as:

$$f_L\,(x) = \sum_{i=1}^{L} \beta_i G\left(W_i^* X_j + b_i\right) = h\,(x)\,\beta, \quad j = 1, \cdots, N \quad (11)$$

whereas $G(\cdot)$ denotes the activation function, X_j signifies the j^{th} instance, W_i represents the input weight, β_i stands for the resultant weight, b_i represents the bias, and $h(x)$ indicates the resultant of HL.

This methodology is utilized for calculating $H^{\dagger}$ (the Moore-Penrose matrix of HL resultant matrix H) is orthographic projection: i.e., once $H^T H$ is non-singular, $H^{\dagger} = (H^T H)^{-1} H^T$, once HH^T is singular, $H^{\dagger} = H^T (HH^T)^{-1}$. Based on the rule of ridge regression, in the computation of $H^{\dagger}$, a lesser positive number $\frac{1}{\lambda}$ is established on the diagonal of HH^T or $H^T H$ as a regularized item that enhances the generalized outcome of ELM. So, during the regularized based ELM:

Once the count of trained instances is superior to the count of HL nodes, the resultant weighted matrix $\hat{\beta}$ is measured by the subsequent formula:

$$\hat{\beta} = \left(\frac{1}{\lambda} + HH^T\right)^{-1} H^T T, N > n_h \quad (12)$$

Or else, once the trained instances counts are lesser than the amount of HL nodes, the resultant weighted matrix $\hat{\beta}$ computation equation as:

$$\hat{\beta} = \left(\frac{1}{\lambda} + HH^T\right)^{-1} H^T T, N > n_h \quad (13)$$

Disassembling the SELM approach is also into several ELM approaches, but all the HL are assumed to be an independent ELM for extracting features. Additionally, to comprehensively reform the input, the ELM gives input as the model target outcome ($i.e., T = X$). The feature learning method for the SELM approach is thorough but the input image can preserved as the target outcome from the primary ELM ($T = X$) for calculating the outcome-weighted matrix β_1 (in red box). Afterward, the outcome of 1st HL $H_1 = \beta_1 \mathrm{x} X$ is provided as the 2nd input and target outcome of ELM ($T = H_1$) for calculating the resultant weighted matrix β_2 (in the green box). At last, it attained a higher-level feature representation $\beta_3 \mathrm{x} H_2$. Therefore, the method develops a linear model, and the resultant weighted matrix of all the ELM β_k is calculated based on the count of HL nodes.

IV. RESULTS AND DISCUSSION

In this part, the performance validation of the CACCD-GOADL technique can be tested employing a medical image database, comprising 918 samples with seven classes such as columnar (CE), Carcinoma In Situ (SCCSI), Mild Dysplasia (MS-NKD), Superficial squamous (SSE), Severe Dysplasia (SS-NKD), Intermediate Squamous (ISE), and Moderate Dysplasia (MOS-NKD). Table 1 signifies the complete details of a dataset.

Fig. 3 displays the confusion matrices produced by the CACCD-GOADL technique at 80:20 and 70:30 of the TRAP/TESP. The simulated values indicate the effectual detection with all seven class labels.

In Table 2 and Fig. 4, the detection analysis of the CACCD-GOADL methodology with 80:20 of TRAP/TESP is provided. The results demonstrate that the CACCD-GOADL method categorizes all 7 samples. With 80% of the TRAP,

TABLE 1. Database details.

Classed	No. of Images
SSE	74
ISE	70
CE	98
MS-NKD	182
MOS-NKD	146
SS-NKD	197
SCCSI	151
Total Images	918

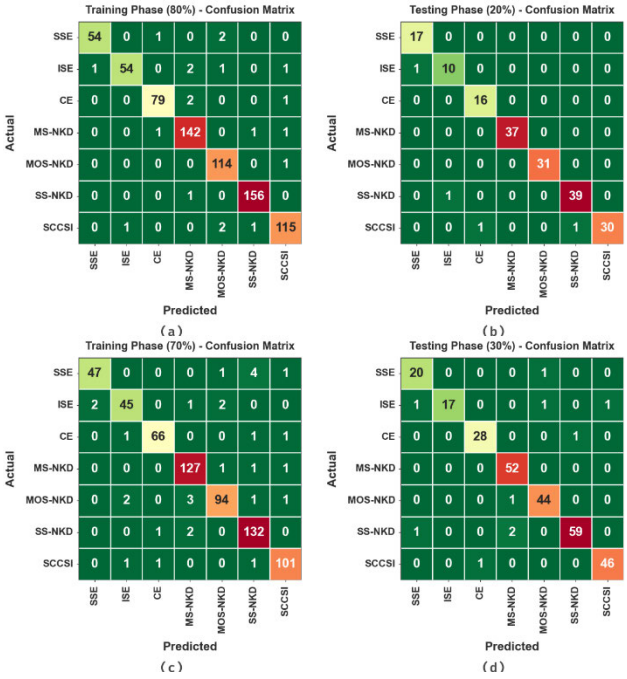

FIGURE 3. Confusion matrices of (a-c) TRAP of 80% and 70% and (b-d) TESP of 20% and 30%.

the CACCD-GOADL system provides an average $accu_y$ of 99.22%, $prec_n$ of 97.38%, $reca_l$ of 96.52%, F_{score} of 96.93%, and MCC of 96.49%. Additionally, based on 20% of the TESP, the CACCD-GOADL methodology gives an average $accu_y$ of 99.38%, $prec_n$ of 96.71%, $reca_l$ of 97.45%, F_{score} of 97.04%, and MCC of 96.71% respectively.

In Table 3 and Fig. 5, the recognition analysis of the CACCD-GOADL methodology with 70:30 of TRAP/TESP is exhibited. The simulated values show that the CACCD-GOADL technique categorizes all 7 samples. According to 70% of the TRAP, the CACCD-GOADL model gives an average $accu_y$ of 98.66%, $prec_n$ of 95.24%, $reca_l$ of 94.28%, F_{score} of 94.73%, and MCC of 93.96%. Moreover, with 30% of TESP, the CACCD-GOADL method provides an average $accu_y$ of 98.96%, $prec_n$ of 96.27%, $reca_l$ of 95.37%, F_{score} of 95.71%, and MCC of 95.17% disparately.

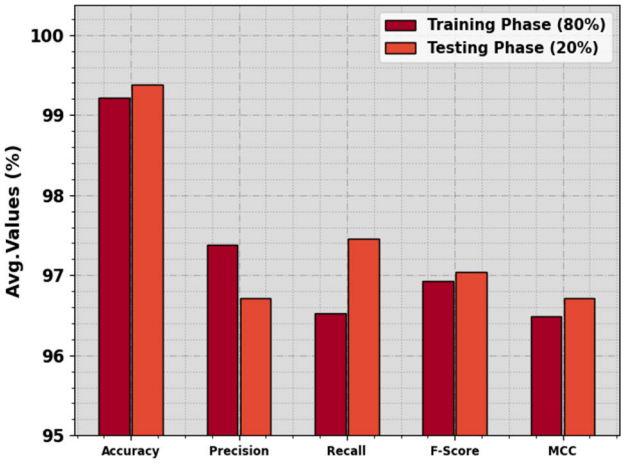

FIGURE 4. Average of CACCD-GOADL algorithm with 80:20 of TRAP/TESP.

TABLE 2. Detection outcome of CACCD-GOADL algorithm with 80:20 of TRAP/TESP.

Class Labels	$Accu_y$	$Prec_n$	$Reca_l$	F_{score}	MCC
TRAP (80%)					
SSE	99.46	98.18	94.74	96.43	96.15
ISE	99.18	98.18	91.53	94.74	94.36
CE	99.32	97.53	96.34	96.93	96.55
MS-NKD	98.91	96.60	97.93	97.26	96.58
MOS-NKD	99.18	95.80	99.13	97.44	96.97
SS-NKD	99.59	98.73	99.36	99.05	98.79
SCCSI	98.91	96.64	96.64	96.64	95.99
Average	99.22	97.38	96.52	96.93	96.49
TESP (20%)					
SSE	99.46	94.44	100.00	97.14	96.89
ISE	98.91	90.91	90.91	90.91	90.33
CE	99.46	94.12	100.00	96.97	96.73
MS-NKD	100.00	100.00	100.00	100.00	100.00
MOS-NKD	100.00	100.00	100.00	100.00	100.00
SS-NKD	98.91	97.50	97.50	97.50	96.81
SCCSI	98.91	100.00	93.75	96.77	96.19
Average	99.38	96.71	97.45	97.04	96.71

To define the performance of the CACCD-GOADL system with 80:20 of TRAP/TESP, TRA, and TES $accu_y$ curves are definite, as demonstrated in Fig. 6. The TRA and TES $accu_y$ curves exhibit the values of the CACCD-GOADL system over numerous epochs. The figure offers important facts regarding the learning tasks and generalized capabilities of the CACCD-GOADL system. With an improvement in epoch count, it is observed that the TRA and TES $accu_y$ curves

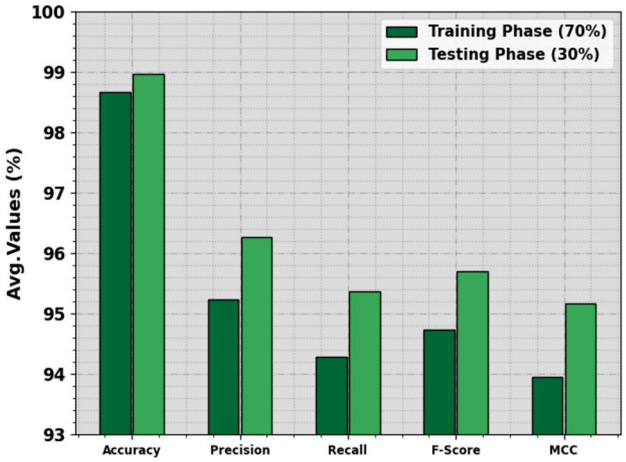

FIGURE 5. Average of CACCD-GOADL algorithm with 70:30 of TRAP/TESP.

TABLE 3. Detection outcome of CACCD-GOADL algorithm with 70:30 of TRAP/TESP.

Class Labels	$Accu_y$	$Prec_n$	$Reca_l$	F_{score}	MCC
TRAP (70%)					
SSE	98.75	95.92	88.68	92.16	91.56
ISE	98.60	91.84	90.00	90.91	90.16
CE	99.22	97.06	95.65	96.35	95.92
MS-NKD	98.60	95.49	97.69	96.58	95.71
MOS-NKD	98.29	95.92	93.07	94.47	93.47
SS-NKD	98.29	94.29	97.78	96.00	94.94
SCCSI	98.91	96.19	97.12	96.65	96.00
Average	98.66	95.24	94.28	94.73	93.96
TESP (30%)					
SSE	98.91	90.91	95.24	93.02	92.46
ISE	98.91	100.00	85.00	91.89	91.66
CE	99.28	96.55	96.55	96.55	96.15
MS-NKD	98.91	94.55	100.00	97.20	96.58
MOS-NKD	98.91	95.65	97.78	96.70	96.06
SS-NKD	98.55	98.33	95.16	96.72	95.81
SCCSI	99.28	97.87	97.87	97.87	97.44
Average	98.96	96.27	95.37	95.71	95.17

acquire enhanced. It is noticed that the CACCD-GOADL methodology attains improved testing accuracy that can potentially recognize the designs in the TRA and TES data.

Fig. 7 represents the complete TRA and TES loss values of the CACCD-GOADL technique with 80:20 of TRAP/TESP over epochs. The TRA loss reported that the method loss attained reduced over epochs. Mostly, the loss values are minimized as the model adjusts the load to reduce the forecast fault on the TRA and TES data. The loss curves display the

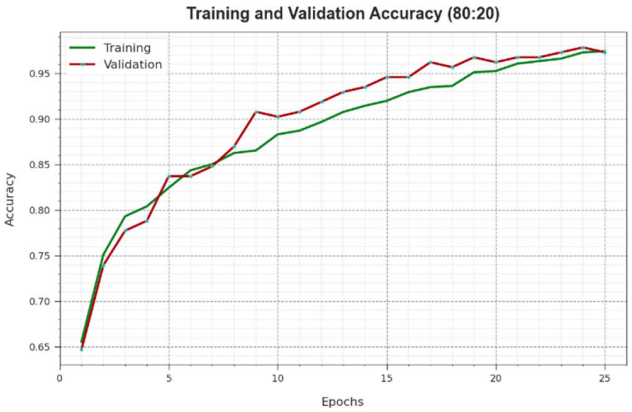

FIGURE 6. $Accu_y$ curve of CACCD-GOADL algorithm with 80:20 of TRAP/TESP.

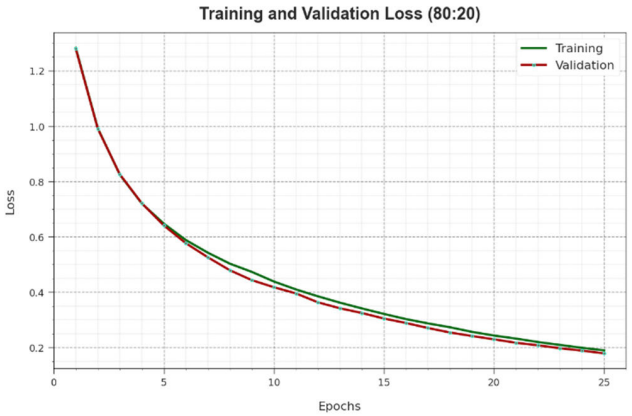

FIGURE 7. Loss curve of CACCD-GOADL algorithm with 80:20 of TRAP/TESP.

level to which the method is suitable for the TRA data. It is evidenced that the TRA and TES loss is gradually reduced and represents that the CACCD-GOADL model successfully learns the designs shown in the TRA and TES data. It is also remarked that the CACCD-GOADL system modified the parameters to decrease the difference amongst the predicted as well as actual TRA labels.

The PR performance of the CACCD-GOADL technique with 80:20 of TRAP/TESP is exhibited to plot accuracy against recall as labeled in Fig. 8. The simulated values confirm that the CACCD-GOADL method achieves improved RR values with all 7 class labels. The figure indicates that the method learns to classify dissimilar classes. The CACCD-GOADL algorithm obtained improved results in the recognition of optimistic samples with reduced false positives.

The ROC study provides the CACCD-GOADL methodology with 80:20 of TRAP/TESP as shown in Fig. 9, which can differentiate the seven classes. The figure specifies respected insights into the tradeoff amongst the TPR and FPR rates over various classification thresholds and modifying the count of epochs. It offers the precise forecast performance of the

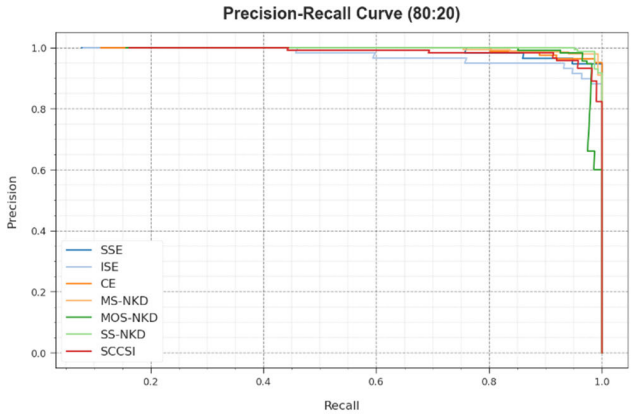

FIGURE 8. PR curve of CACCD-GOADL algorithm with 80:20 of TRAP /TESP.

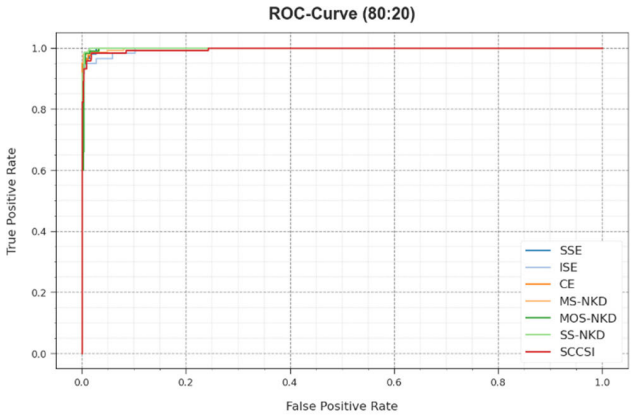

FIGURE 9. ROC curve of CACCD-GOADL algorithm with 80:20 of TRAP/TESP.

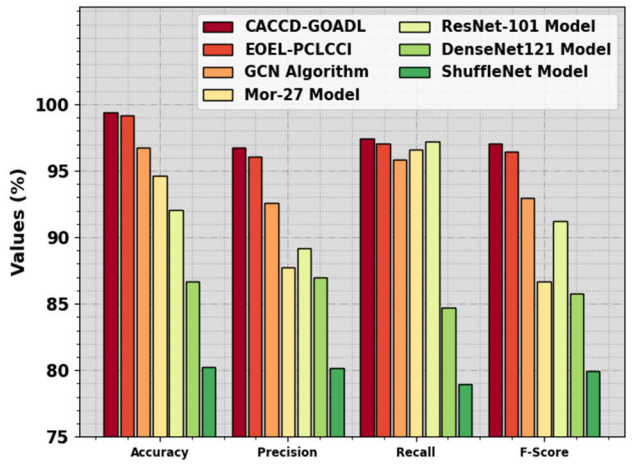

FIGURE 10. Comparative outcome of CACCD-GOADL algorithm with other recent systems.

CACCD-GOADL methodology on the recognition of diverse 7 class labels.

In Table 4 and Fig. 10, a contrast study of the CACCD-GOADL approach with recent systems [26], [27]. It is noticed that the DenseNet121 and ShuffleNet models have shown worse results. In addition, the GCN, Mor-27, and ResNet-101 models have obtained considerable performance. At the same time, the EOEL-PCLCCI model reaches reasonable performance. The results indicate that the CACCD-GOADL algorithm reaches enhanced results with maximum performance with maximum $accu_y$ of 99.38%, $prec_n$ of 96.71%, $reca_l$ of 97.45%, and F_{score} of 97.04%. These results show excellent performance of the CACCD-GOADL technique.

TABLE 4. Comparative outcome of CACCD-GOADL algorithm with other recent systems.

Methods	$Accu_y$	$Prec_n$	$Reca_l$	F_{score}
CACCD-GOADL	99.38	96.71	97.45	97.04
EOEL-PCLCCI	99.17	96.02	97.05	96.46
GCN Algorithm	96.74	92.58	95.85	92.93
Mor-27 Model	94.59	87.75	96.57	86.69
ResNet-101 Model	92.01	89.18	97.21	91.21
DenseNet121 Model	86.71	86.95	84.71	85.74
ShuffleNet Model	80.25	80.18	78.96	79.97

V. CONCLUSION

In this research paper, we have mainly concentrated on the design and growth of an automated CACCD-GOADL technique for the identification and recognition of CC. The main intention of the CACCD-GOADL methodology is to inspect the image detection of CC. To accomplish this, the CACCD-GOADL approach incorporates an improved MobileNetv3 model, GOA-based hyperparameter tuning, and SELM classification. Moreover, the CACCD-GOADL technique designs a new GOA for the hyperparameter tuning of the improved MobileNetv3 system. For the identification and detection of cancer, the CACCD-GOADL methodology used the SELM technique. The simulation validation of the CACCD-GOADL methodology is verified on the benchmark dataset of Herlev. A comparison of outcomes depicted that the CACCD-GOADL system reaches superior outcomes with other approaches.

The significance of these findings is underscored by the superior outcomes demonstrated in the evaluation of the benchmark Herlev dataset, suggesting its potential to enhance the accuracy and efficiency of cervical cancer detection. Furthermore, the CACCD-GOADL framework holds promising implications for clinical practice, offering a reliable and automated diagnostic tool that could augment the capabilities of healthcare professionals in cervical cancer screening. The incorporation of artificial intelligence and deep learning in this approach has the potential to reduce human error and improve the overall reliability of diagnostic outcomes. The success of CACCD-GOADL also points toward avenues for further research, encouraging exploration into optimizing and

expanding the framework for broader applications in medical imaging and diagnostic methodologies. The holistic nature of the approach positions it as a noteworthy advancement with substantial implications for advancing cervical cancer diagnosis and potentially reshaping the landscape of automated diagnostic tools in healthcare.

ACKNOWLEDGMENT

The authors would like to thank Deputy Deanship for Research and Innovation, Ministry of Education in Saudi Arabia for funding this research work through the under Project IFP22UQU4310373DSR183.

REFERENCES

[1] P. Xue, J. Wang, D. Qin, H. Yan, Y. Qu, S. Seery, Y. Jiang, and Y. Qiao, "Deep learning in image-based breast and cervical cancer detection: A systematic review and meta-analysis," *NPJ Digit. Med.*, vol. 5, no. 1, p. 19, Feb. 2022.

[2] N. Wentzensen, B. Lahrmann, M. A. Clarke, W. Kinney, D. Tokugawa, N. Poitras, A. Locke, L. Bartels, A. Krauthoff, J. Walker, and R. Zuna, "Accuracy and efficiency of deep-learning–based automation of dual stain cytology in cervical cancer screening," *J. Nat. Cancer Inst.*, vol. 113, no. 1, pp. 72–79, 2021.

[3] M. Mehmood, M. Rizwan, M. G. Ml, and S. Abbas, "Machine learning assisted cervical cancer detection," *Frontiers Public Health*, vol. 9, Dec. 2021, Art. no. 788376.

[4] I. Syed, B. R. Altahan, S. H. Ahammad, V. Rajesh, R. R. Kalangi, L. K. Smirani, M. A. Hossain, and A. N. Z. Rashed, "Skin disease detection using deep learning," *Adv. Eng. Softw.*, vol. 175, Jan. 2023, Art. no. 103361.

[5] H. Chen, J. Liu, Q.-M. Wen, Z.-Q. Zuo, J.-S. Liu, J. Feng, B.-C. Pang, and D. Xiao, "CytoBrain: Cervical cancer screening system based on deep learning technology," *J. Comput. Sci. Technol.*, vol. 36, no. 2, pp. 347–360, Apr. 2021.

[6] A. Aljarf, G. Almaghrabi, H. Albarakati, H. Ahmed, R. Alharbi, and S. Aljuhani, "EBSAR: Detecting of objects that hinder visually impaired in a controlled area using deep learning," in *Proc. 5th Nat. Conf. Saudi Comput. Colleges (NCCC)*, Makkah, Saudi Arabia, Dec. 2022, pp. 19–25, doi: 10.1109/NCCC57165.2022.10067421.

[7] F. Kanavati, N. Hirose, T. Ishii, A. Fukuda, S. Ichihara, and M. Tsuneki, "A deep learning model for cervical cancer screening on liquid-based cytology specimens in whole slide images," *Cancers*, vol. 14, no. 5, p. 1159, Feb. 2022.

[8] K. T. Desai, B. Befano, Z. Xue, H. Kelly, N. G. Campos, D. Egemen, J. C. Gage, A. Rodriguez, V. Sahasrabuddhe, D. Levitz, P. Pearlman, J. Jeronimo, S. Antani, M. Schiffman, and S. de Sanjosé, "The development of 'automated visual evaluation' for cervical cancer screening: The promise and challenges in adapting deep-learning for clinical testing," *Int. J. Cancer*, vol. 150, no. 5, pp. 741–752, Mar. 2022.

[9] U. K. Lilhore, M. Poongodi, A. Kaur, S. Simaiya, A. D. Algarni, H. Elmannai, V. Vijayakumar, G. B. Tunze, and M. Hamdi, "Hybrid model for detection of cervical cancer using causal analysis and machine learning techniques," *Comput. Math. Methods Med.*, vol. 2022, pp. 1–17, May 2022.

[10] M. Yu, M. Han, X. Li, X. Wei, H. Jiang, H. Chen, and R. Yu, "Adaptive soft erasure with edge self-attention for weakly supervised semantic segmentation: Thyroid ultrasound image case study," *Comput. Biol. Med.*, vol. 144, May 2022, Art. no. 105347.

[11] Y. Chen, X. H. Yang, Z. Wei, A. A. Heidari, and N. Zheng, "Generative adversarial networks in medical image augmentation: A review," *Comput. Biol. Med.*, vol. 144, Jan. 2022, Art. no. 105382.

[12] M. I. Waly, M. Y. Sikkandar, M. A. Aboamer, S. Kadry, and O. Thinnukool, "Optimal deep convolution neural network for cervical cancer diagnosis model," *Comput., Mater. Continua*, vol. 70, no. 2, pp. 3295–3309, 2022.

[13] A. Bhargava, P. Gairola, G. Vyas, and A. Bhan, "Computer aided diagnosis of cervical cancer using HoG features and multi classifiers," in *Intelligent Communication, Control and Devices*. Singapore: Springer, 2017, pp. 1491–1502.

[14] Z. Karapinar and S. Uzun, "An improved deep learning based cervical cancer detection using a median filter based preprocessing," *Eur. J. Sci. Technol.*, vol. 30, pp. 50–58, Jan. 2022.

[15] C. Suguna and S. P. Balamurugan, "Computer aided diagnosis for cervical cancer screening using monarch butterfly optimization with deep learning model," in *Proc. 5th Int. Conf. Smart Syst. Inventive Technol. (ICSSIT)*, Jan. 2023, pp. 1059–1064.

[16] R. Elakkiya, K. S. S. Teja, and L. J. Deborah, "Imaging based cervical cancer diagnostics using small object detection-generative adversarial networks," *Multimedia Tools Appl.*, vol. 2022, pp. 1–17, Jan. 2022.

[17] A. N. A. Masri and H. Mokayed, "An efficient machine learning-based cervical cancer detection and classification," *J. Cybersecur. Inf. Manage.*, vol. 2, no. 2, pp. 8–58, 2021.

[18] C. Li, D. Xue, X. Zhou, J. Zhang, H. Zhang, Y. Yao, F. Kong, L. Zhang, and H. Sun, "Transfer learning based classification of cervical cancer immunohistochemistry images," in *Proc. 3rd Int. Symp. Image Comput. Digit. Med.*, Aug. 2019, pp. 102–106.

[19] Z. Alyafeai and L. Ghouti, "A fully-automated deep learning pipeline for cervical cancer classification," *Expert Syst. Appl.*, vol. 141, Mar. 2020, Art. no. 112951.

[20] Q. Guan, Y. Chen, Z. Wei, A. A. Heidari, H. Hu, X.-H. Yang, J. Zheng, Q. Zhou, H. Chen, and F. Chen, "Medical image augmentation for lesion detection using a texture-constrained multichannel progressive GAN," *Comput. Biol. Med.*, vol. 145, Jun. 2022, Art. no. 105444.

[21] G.-Q. Zhou, W.-B. Zhang, Z.-Q. Shi, Z.-R. Qi, K.-N. Wang, H. Song, J. Yao, and Y. Chen, "DSANet: Dual-branch shape-aware network for echocardiography segmentation in apical views," *IEEE J. Biomed. Health Informat.*, 2023.

[22] K.-N. Wang, X. Yang, J. Miao, L. Li, J. Yao, P. Zhou, W. Xue, G.-Q. Zhou, X. Zhuang, and D. Ni, "AWSnet: An auto-weighted supervision attention network for myocardial scar and edema segmentation in multi-sequence cardiac magnetic resonance images," *Med. Image Anal.*, vol. 77, Apr. 2022, Art. no. 102362.

[23] Y. Yuldashev, M. Mukhiddinov, A. B. Abdusalomov, R. Nasimov, and J. Cho, "Parking lot occupancy detection with improved MobileNetV3," *Sensors*, vol. 23, no. 17, p. 7642, Sep. 2023.

[24] S. Ekinci and D. Izci, "Enhancing IIR system identification: Harnessing the synergy of gazelle optimization and simulated annealing algorithms," *E-Prime-Adv. Electr. Eng., Electron. Energy*, vol. 5, Sep. 2023, Art. no. 100225.

[25] J. Yang, W. Sun, N. Liu, Y. Chen, Y. Wang, and S. Han, "A novel multimodal biometrics recognition model based on stacked ELM and CCA methods," *Symmetry*, vol. 10, no. 4, p. 96, 2018.

[26] R. A. Mansouri and M. Ragab, "Equilibrium optimization algorithm with ensemble learning based cervical precancerous lesion classification model," *Healthcare*, vol. 11, no. 1, p. 55, Dec. 2022.

[27] S. Fang, J. Yang, M. Wang, C. Liu, and S. Liu, "An improved image classification method for cervical precancerous lesions based on ShuffleNet," *Comput. Intell. Neurosci.*, vol. 2022, pp. 1–8, Sep. 2022.